scientific reports



OPEN

Machine learning investigation of marangoni convection in hybrid nanofluids with Darcy-Forchheimer

Hamid Qureshi¹, Sebastian Altmeyer^{®2™} & Muhammad Zubair³

This research utilizes machine learning to investigate Marangoni convection in a hybrid nanofluid $(MnZnFe_2O_4+NiZnFe_2O_4/H_2O)$ within a Darcy-Forchheimer porous framework. We conduct both qualitative and quantitative assessments of heat transfer, mass transfer, and viscous dissipation irreversibility during the flow. Numerical results are obtained using a Python finite difference algorithm, after which MATLAB is employed for Al-based analysis. Additionally, the Levenberg–Marquardt neural network algorithm is trained and utilized. Our findings show that fluid velocity diminishes as the inverse Darcy parameter, Marangoni ratio, and Forchheimer parameter increase. Moreover, the temperature rises with the Eckert number and Prandtl ratio. As concentration increases, activation energy and Schmidt parameter also grow. Mean Square Error for the results reaches up to 10^{-11} across various impacts. The findings indicate that the LMNN model fits well with low error in training, testing and validation dataset. Notably, the results indicate that this hybrid Al-based method could be used as a credible surrogate of the intricate simulations in porous media heat transfer tasks providing a computationally effective device of real-time analysis in engineering.

Keywords Artificial intelligence, Machine learning, Levenberg Marquardt neural-network algorithm, Hybrid nanofluid, Darcy Forchheimer, Marangoni ratio, Convection

The field of heat transfer is garnering increasing attention due to two primary reasons: the pursuit of understanding its foundational principles and the industrial opportunities offered by conduction, convection, and radiation to improve thermal management systems. Considerable efforts are aimed at discovering methods to boost heat transfer efficacy, as it plays a pivotal role in designing and executing projects. Convective flow 1 involves fluid motion where heat transfer arises from changes in density and temperature. In this mechanism, warmer, lighter fluid rises while cooler, denser fluid sinks, creating a circulation that enhances heat distribution². This process is essential to numerous natural and industrial phenomena, including global weather systems, ocean currents, and cooling of electronic devices. Figure 1 depicts various sector-wide applications. Mastery of convective flow is essential for scientists and engineers focused on refining climate models, enhancing industrial processes, and developing sustainable heating and cooling solutions. Thermocapillary convection, known also as Marangoni convective flow^{3,4}, emerges in fluid dynamics when surface tension varies along an interface, typically owing to temperature or concentration differentials. This phenomenon is crucial in numerous natural and industrial contexts, like crystal growth, microfluidic systems, and thin film production. The fluid shifts from regions of low to high surface tension due to non-uniform surface tension, producing intricate flow patterns that can either improve or obstruct heat and mass transfer. Thus, managing and adjusting Marangoni convective flow is essential to optimizing results in fields such as materials science and biotechnology.

Nanofluids^{2,3} or ferrofluids^{4–6} are a novel way to enhance thermal properties and efficiency of heat transfer. They are developed through the inclusion of nano-meter-sized particles (less than 100 nm) in a base liquid carrier fluid. These particles can significantly improve the thermal conductivity and stability of common fluids, e.g., oils, water, or ethylene alcohol⁷. Hybrid nano-fluids⁸, a modification of traditional nanofluids, are fluids that contain two or more different types of nanoparticles. Their performance is influenced by both particle size and base fluid, leading to a reduction in thermal conductivity; Meanwhile, physical properties such as surface tension or flow field may also fall within what is allowed of both sides' ranges for outperforming single-component nano-fluids in many new fields. In particular, the often-detected disadvantages due to viscosity may be eliminated in many cases. These advantages are caused by the fact that there are two assorted sizes and composition rates involved. The influence between each other is small and therefore several disadvantages are overcome, especially when

¹Department of Mathematics, Mohi-Ud-Din Islamic University, Nerian Sharif, AJK, Pakistan. ²Universitat Politecnica de Catalunya EETAC - School of Telecom and Aerospace Engineering, Barcelona, Spain. ³School of Qilu Transportation, Shandong University, Jinan 250061, China. [™]email: sebastian.andreas.altmeyer@upc.edu



Fig. 1. Applications of Nanofluids⁵⁵.

considering limitations analogous to Moore's Law (empirical law predicting that microchip transistor counts would double every two years and therefore boosting computing power while lowering costs) in computational scaling. Hybrid nanofluids exhibit superior thermal properties compared to traditional coolants and lubricants.

This study explored optimal combinations and concentrations of nano-fillers to develop hybrid nanofluids aimed at enhancing heat transfer performance. Ahmad et al. investigated nonlinear hybrid nano-fluids⁹, while Buongiorno¹⁰ introduced a two-phase thermal energy transport model based on nano-fluids. Tiwari and Das¹¹ proposed a mathematical model that factors in the thermophysical properties and volumeric fraction function of nanoparticles. Pordanjani et al. 12 offer a critical review of nano-fluids, examining their physical attributes, applications in thermal systems, environmental concerns, and heat transfer effectiveness, alongside potential environmental issues and future research paths. Liu et al. 13 employed numerical techniques to study bio-convective phenomena in rate-type nano-fluids. Various studies highlight the potential and computational models of nano-fluids across engineering fields, underscoring their ability to enhance efficiency 14-17. Significant research contributions to nano-fluidic systems have been made by J. Wang¹⁸, A. I. Alsabery¹⁹, Khan²⁰, S. K. Patel²¹, A. M. Saeed²², and S. Li²³. Recent analyses have focused on nanofluid and hybrid nanofluid flows, evaluating heat and mass transfer under diverse physical phenomena like radiation, magnetohydrodynamics, and chemical reactions 10,14,24-32. Several numerical studies and review papers have addressed nanofluid stability and thermal performance enhancement through hybrid nanoparticle use^{20,31-33}, with similar models being numerically investigated in^{34,35}. Shehzad et al.³⁶ examined the convective magnetohydrodynamic (MHD) flow of a hybrid nano-fluid contained by an elliptic porous wall, analyzing fluid dynamics and heat transfer's impact on porosity and magnetic fields. Radhika³⁷ utilized advanced mathematical modeling and simulation to analyze the improved heat transfer properties of dusty fluids with suspended hybrid nanoparticles over a melting surface. Collectively, these studies underscore the potential of hybrid nano-fluids for boosting heat transfer and fluid dynamics in engineering applications, with detailed numerical analyses under various physical conditions like thermal radiation 10,14,24,25, MHD effects, and different geometrical and boundary conditions 27,29,36,38-40.

To date, in the field of computational fluid mechanics, researchers mostly focus on deterministic numerical or analytical techniques. However, recent developments open the door to comparatively less explored stochastic numerical computing solvers based on artificial intelligence (AI) approaches, particularly nano-fluidic models. The computational capabilities of stochastic numerical computing solvers based on AI with neural networks to solve linear and non-linear differential equations are used to address different problems arising in several domains. In the modern era, Shah et al.⁴¹ enhanced predictive accuracy in complex fluid scenarios by implementing a neural network-based evaluation technique for the numerical analysis of the flow of an Eyring-Powell magneto nano-fluidic structure. Different works have proven how to use computational intelligence methods to analyze different fluid models, such as those involving convective flows, magneto-nano-fluids, and nano-fluids. Several works also analyzed intricate fluid behavior and optimized design parameters in engineering applications 42-45. A unified trend with a focus on applying sophisticated computational techniques can be seen. This includes machine learning and stochastic networks to analyze and optimize fluid flow models involving bio-convection and nano-fluids. This reflects the growing significance of computational intelligence in a variety of engineering applications. 46,49,68. Gowtham and Keerthi^{50–53} investigated third-grade and hybrid fluids for various geometries. In recent years, the effectiveness of neural-network-based methods to understand complex non-Newtonian, hybrid nanofluids in a wide variety of physical regimes, such as Kelvin Voigt fluid modeling⁵⁴, hybrid nanofluids transport in converging/diverging channels⁵⁵, Arrhenius activation energies and thermal radiation effects⁵⁶, hydromagnetic convection in porous channels⁵⁷, and ternary hybrid nanofluid particle deposition⁵⁸, have been shown. Artificial neural networks based on Levenberg-Marquardt have recently been used to model a wide variety of non-Newtonian and nanofluid flows, such as transient micropolar nanofluid microchannel flow⁵⁹, Casson-Carreau nanofluid transport over curved surfaces⁶⁰, radiative Casson fluid flow with couple stresses⁶¹, Prandtl fluid dynamics over stratified geometries⁶², and optimization of dusty-trihybrid nanofluid microchannel flows using ANOVA-Taguchi methods⁶³. Recent reports have emphasized some of the practical uses of nanofluid systems, such as ionic water/ graphene nanofluids in solar panels⁶⁴, conjugate mixed convection of hybrid ethylene glycol nanoparticles with Joule heating⁶⁵, optimization of heat transfer in MWCNT-Al2O3 hybrid nanofluids⁶⁶, and graphene oxide/vacuum residue nanofluids in enhanced oil recovery⁶⁷.

The flow system features a two-dimensional steady-state setup in which a hybrid nanofluid interacts with a porous surface that has distinct temperature and concentration regions. The model requires boundary conditions that include fully adhering velocity and specified thermal and mass transfer rates. The integration of dual nanoparticles $(MnZnFe_2O_4+NiZnFe_2O_4/H_2O)$ together with AI-driven stochastic modeling represents the novelty because it fills the prediction gaps for thermocapillary-driven flows in porous media.

The primary components of the research methodology are outlined as follows:

- AI-driven methods were utilized to generate tailored outputs for numerical studies within the Darcy-Forchheimer model framework.
- The mathematical model, which is generally non-linear, consists of coupled partial differential equations (PDEs). Through the application of similarity variables, these PDEs are converted into a set of equivalent non-linear ordinary differential equations (ODEs).
- An in-depth analysis and study of the model were conducted using a Python algorithm. Key parameters
 examined include the Darcy parameter, Marangoni fraction, Forchheimer parameter, Eckert ratio, Prandtl
 number, energy characteristic, and Schmidt number.
- The proposed Python-based machine learning computational approach was validated via extensive testing, training, and validation processes, modeling fluid behavior under different conditions, and benchmarking against existing data.
- The Mean Squared Error (MSE) merit function was employed to verify the method's effectiveness in addressing the model, supplemented by analyses of histograms and convergence plots.
- Comprehensive Training, Testing, and Validation (TTV) of the convergence parameter of LMNA across various stages has been undertaken.

Comparison with previous reviews

Initiating with a recognition of early research on Marangoni convection and hybrid nanofluids, particularly those utilizing computational approaches, is essential. For instance, it's possible to cite approaches by Ahmad et al. and Buongiorno et al. 9,10, among others, which were regarded in their studies but not directly compared. Highlight the methodological distinctions in developing a Darcy-Forchheimer porous medium concentrating on MnZnFe₂O₄ and NiZnFe₂O₄ nanoparticles, which have not been explored in other research.

Previous studies have employed neural networks, genetic algorithms, and hybrid AI solutions to forecast nanofluids' thermal and mass transfer properties $^{45-48}$, yet none have integrated MnZnFe $_2$ O $_4$ -NiZnFe $_2$ O $_4$ -Nybrid nanoparticles within a Darcy–Forchheimer porous medium influenced by Marangoni convection. Furthermore, prior machine learning applications were confined to limited parametric scopes, whereas this research symmetrically assesses the Darcy, Forchheimer, Prandtl, and Eckert numbers under thermocapillary conditions. Additionally, the ferrite-based nanoparticles offer improved magneto-thermal properties, setting our study apart from those focusing on oxide-based nanofluids.

Identifying research gaps

This research seeks to examine the existing constraints in the investigation of Marangoni convection and the novel applications of hybrid nanofluids that it intends to overcome. Unlike previous studies that have depended heavily on deterministic numerical techniques, this research introduces a stochastic, AI-driven approach focusing on probabilities and sensitivities. Highlight the specific parameters or conditions analyzed; for example, how machine learning influences fluid dynamics through various thermophysical properties. This distinction could illuminate AI's potential to address computational or modeling difficulties typically encountered in conventional hybrid nanofluid studies.

Explicit contribution statement

The research reveals important findings regarding how the combined dependence of ξ and η influences heat and mass transfer in hybrid nanofluids experiencing Marangoni convection. It recommends employing the Levenberg–Marquardt Neural Network Algorithm to boost prediction accuracy. These findings set the stage for further research into complex geometries, variable flow dynamics, and multi-phase phenomena, thereby expanding the reach of our predictive models. The paper highlights practical applications, particularly in microelectronics cooling, optimizing heat exchangers, and improving renewable energy systems.

Mathematical modeling Governing equations

Consider the heat and mass transfer from a higher surface pressure to a lower surface pressure inside a hybrid nanofluid. Here, we assume an incompressible, steady flow of a hybrid nano-fluid with a composition of nanoparticles of Manganese Zinc Ferrite and Nickel Zinc Ferrite $(MnZnFe_2O_4 + NiZnFe_2O_4)$ with water as a base fluid, as an excellent dispersant, and non-toxic. These ferrites have enhanced magnetic properties and thermal conductance. Entropy generation, viscous dissipation, and the impact of Darcy-Forchheimer permeable medium are considered. Modeled equations based on the aforementioned assumptions are as follows⁷⁻¹⁰. References for Eqs. (1) to (5), including further background information, can be found in ^{5,9}.

$$\frac{\partial u}{\partial x} + \frac{\partial v}{\partial y} = 0 \tag{1}$$

$$u\left(\frac{\partial u}{\partial x}\right) + v\left(\frac{\partial v}{\partial y}\right) + \frac{v_{hnf}}{K^*}u + Fu^2 = \left(\frac{\mu_{hnf}}{\rho_{hnf}}\right)\left(\frac{\partial^2 u}{\partial y^2}\right) \tag{2}$$

$$u\left(\frac{\partial T}{\partial x}\right) + v\left(\frac{\partial T}{\partial y}\right) - \frac{k_{hnf}}{(\rho c_p)_{hnf}}\left(\frac{\partial^2 T}{\partial y^2}\right) = \frac{\mu_{hnf}}{(\rho c_p)_{hnf}}\left(\frac{\partial u}{\partial y}\right)^2 \tag{3}$$

$$u\left(\frac{\partial C}{\partial x}\right) + v\left(\frac{\partial C}{\partial y}\right) + k_0^2 \left(C - D_\infty\right) \left(\frac{T}{T_\infty}\right)^n \exp\left(\frac{-E_a}{kT}\right) = D\left(\frac{\partial^2 C}{\partial y^2}\right) \tag{4}$$

$$\mu \frac{\partial u}{\partial z} = \frac{\partial \sigma}{\partial x} = \sigma_0 \left(\gamma_c \left. \frac{\partial C}{\partial x} \right|_{y=0} + \gamma_T \left. \frac{\partial T}{\partial x} \right|_{y=0} \right) \tag{5}$$

Boundary conditions

We use the following boundary conditions (BC) in space and temperature:

$$v = 0, T = T_W T_0 X^2$$
 when $y = 0$ (6)

$$u = 0, T - T_{\infty} = 0, C - C_{\infty} = 0 \text{ if } y \to \infty$$

$$(7)$$

$$\sigma = \sigma_0 \left(1 - \gamma_T \gamma_C \left(T - T_\infty \right) \left(C - C_\infty \right) \right), \tag{8}$$

with initially and more general

$$\gamma_T = \frac{-1}{\sigma_0} \frac{\partial \sigma}{\partial T} \text{ for } T \to \infty \text{ and } \gamma_C = \frac{-1}{\sigma_0} \frac{\partial \sigma}{\partial C} \text{ for } C \to \infty$$
(9)

A schematic illustration of the problem is presented in Fig. 2.

Here, γ_T and γ_C are constants for temperature and concentration. κ is Boltzmann number and surface tension are represented by σ . Activation energy is presented by E_a . However, T_0, T_∞, C_0 and C_∞ represents reference and ambient temperature and concentrations, respectively. $(\rho c_p)_{hnf}$ and k_{hnf} shows heat capacity and thermal conductivity of hybrid nanofluid while, c_p is specific heat capacity. Chemical reaction rate k_0 and permeability of porous medium K^* . Mas diffusivity is symbolized by D, and dynamic viscosity is presented by μ_{hnf} . ρ is the density and (x,y) are the coordinates of the axis.

Similarity equations

In order to non-dimensionalize the governing equations and thus to transform the above system of PDEs into a non-dimensionalized system of ODEs the following similarity variables are introduced (utilizing symmetries and scaling properties):

$$u = \frac{v_f}{L} X f'(\xi), v = \frac{v_f}{L} X f(\xi), \xi = \frac{y}{L}, X = \frac{x}{L}, \theta(\xi) = \frac{T - T_{\infty}}{T_0 X^2}, \phi(\xi) = \frac{C - C_{\infty}}{C_0 X^2}$$
(10)

Equation (1) is satisfied insignificantly, and the remaining Eqs. (2)-(4) transform as follows:

$$f''(\xi) = (1 - \sigma_1)^{2.5} (1 - \sigma_2)^{2.5} A_1 \left((f')^2 - f f'' F_r (f')^2 \right) + (f'),$$
(11)

$$\theta''(\xi) = \frac{A_2 \Pr}{A_3} \left(2\theta' f - \theta f' - \frac{E_c (f')^2}{(1 - \sigma_1)^{2.5} (1 - \sigma_2)^{2.5} A_2} \right), \tag{12}$$

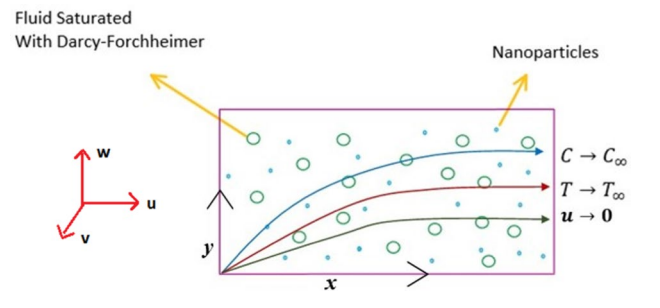


Fig. 2. Spatial Setup of the problem.

Material	$ ho\left(kg/m^3 ight)$	$C_{p}\left(J/\left(kgK_{0} ight) ight) / c$	nKK)
H_2O	997.1	4179	0.613
MnZn Fe_2o_4	4700	1050	3.9
NiZn Fe_2o_4	4800	710	6.3

Table 1. Thermo-physical properties of HNFs⁵⁵.

Parameter	Relation
Inverse Darcy coefficient	$B = \frac{v_f L^2}{K^* \sigma_f}$
Forchheimer parameter	$F_r = \frac{C_b}{\sqrt{K^*}}$
Prandtl ratio	$\Pr = \frac{v_f}{\sigma_f}$
Schmidt parameter	$Sc = \frac{v_f}{D_f}$
Chemical reaction rate	$k_1 = \frac{k_0^2 L^2}{v_f}$
Activation energy coefficient	$E = \frac{E_0}{kT_{\infty}}$
Temperature coefficient	$\delta = \frac{T_0 X^2}{T_{\infty}}$
Brinkmann parameter	$Br = \frac{\mu v_f^2}{kT_0 L^2 X^2}$
Diffusion constant	$L^* = \frac{R^* DC_0}{k_f}$
Eckert ratio	$Ec = \frac{v_f^2}{c_p T_0 L^2 X^2}$
Concentration coefficient	$\delta_1 = \frac{C_0 X^2}{C_\infty}$
Marangoni parameter	$r = \frac{\gamma_C C_0}{\gamma_T T_0}$

Table 2. Thermo-physical parameters and their formulas⁵⁵. Note that σ_1 and σ_2 are volumetric concentrations of each type of nano-solute.

$$\phi'(\xi) = Sc\left(k_1\left(\delta\theta + 1\right)^n \exp\left(\frac{-E_1}{\delta\theta + 1}\right)\psi' + 2\phi f' - \phi' f\right),\tag{13}$$

Accordingly, the new transformed BCs read:

$$f = 0, f'' = -2(1+r)(1-\sigma_1)^{2.5}(1-\sigma_2)^{2.5}, \theta = 1, \phi = 1 \text{ at } \xi = 0 \text{ and}$$

$$f' = 0, \theta = 0, \phi = 0 \text{ when } \xi \to \infty,$$
 (14)

Thermo-physical properties and characteristics of significant parameters for NF and HNF are listed in Table. 1^{54,55}. Moreover, significant dimensionless parameters and their relations which are involved in the Eqns. (11, 12, 13) and boundary conditions Eq. (14) are listed in Table 2.

Further, the dimensionless Skin Friction and Nusselt numbers are,

$$C_{fx}\sqrt{\text{Re}} = \frac{f''(0)}{\sqrt[5]{(1-\sigma_1)(1-\sigma_2)}} \text{ and } \frac{Nu_x}{\sqrt{\text{Re}}} = -A_4\left(\frac{k_{hnf}}{k_{nf}}\right)\theta'(0)$$
(15)

Following the relations of Entropy and Bejan numbers in dimensionless form are,

$$N_G = A_3 \delta \theta'^2 + \frac{Br \text{Re}}{\sqrt{((1 - \sigma_1)(1 - \sigma_2))^5}} f''^2 + L^* \left(\theta' \phi' + \frac{\delta_1 \phi'^2}{\delta} \right), \tag{16}$$

$$Be = \frac{1}{N_G} \left(A_3 \delta \theta'^2 + L^* \left(\theta' \phi' + \frac{\delta \phi'^2}{\delta} \right) \right), \tag{17}$$

Here, we have from⁵⁵,

$$A_1 = \frac{\rho_{hnf}}{\rho_f} = (1 - \sigma_2) \left((1 - \sigma_1) + \frac{\rho_{s1}}{\rho_f} \right) + \sigma_2 \frac{\rho_{s2}}{\rho_f}, \tag{18}$$

$$A_2 = \frac{(\rho c_p)_{hnf}}{(\rho c_p)_f} = (1 - \sigma_2) \left((1 - \sigma_1) + \sigma_1 \frac{(\rho c_p)_{s1}}{(\rho c_p)_f} \right) + \sigma_2 \frac{(\rho c_p)_{s2}}{(\rho c_p)_f}, \tag{19}$$

$$A_3 = \frac{k_{hnf}}{k_f},\tag{20}$$

$$\frac{k_{hnf}}{k_{nf}} = \frac{k_{s2} - 2\sigma_2 (k_{nf} - k_{s2}) + 2k_{nf}}{k_{s2} + 2\sigma_2 (k_{nf} - k_{s2}) + 2k_{nf}},$$
(21)

$$\frac{k_{nf}}{k_f} = \frac{k_{s1} + 2k_f - \sigma_1 (k_f - k_{s1})}{k_{s1} + 2k_f + \sigma_1 (k_f - k_{s1})},$$
(22)

$$\frac{\mu_{hnf}}{\mu_f} = \frac{1}{\sqrt{((1-\sigma_1)(1-\sigma_2))^5}}$$
 (23)

Some of the significant parameters and their relations are mentioned in Table 2.

Solution methodology

In this research, we employed an original approach for modeling Marangoni convection in hybrid nanofluids, utilizing Python data generation enhanced by a MATLAB Levenberg–Marquardt backpropagation neural network algorithm. While other methods may focus on the general utilization of built-in toolboxes, this system enhances data preprocessing, parameter optimization, and model design in response to the difficult thermophysical relations and disparate nanofluid movement. To reduce the over-fitting problem, cross-validation was used to partition the data into training data (70%), validation data (15%), and test data (15%), and early stopping was used to stop training when the model began to fit the noise. Such a measured incorporation of tools and strategies enabled us to capture convective behaviors of reasonable complexity in more complex hybrid nanofluids accurately, proving that our tailored approach to fluid dynamic modeling is not only efficient but highly specific as well.

In the current study, we describe a novel approach to employing mean variability in the use of machine learning. Thereby, we form a fused environment to compute nonlinear PDEs by developing an innovative fluid flow model for improving HNF ($MnZnFe_2O_4 + NiZnFe_2O_4 + H_2O$) applications for Darcy Forchheimer operating over a porous phase. The particular nano solutes investigated here are Manganese Zinc Ferrite and Nickel Zinc Ferrite.

An implicit Crank-Nicolson finite difference scheme was used to discretize the governing PDEs, since it is stable in stiff nonlinear systems. The grid independence was checked by testing 100, 150, 200, and 250 grid points; after 200, the variations in Nusselt and Sherwood numbers were less than 0.5%. The Courant-Friedrichs-Lewy (CFL) condition was used to ensure stability, and convergence was proclaimed when the successive iterations met the condition of |human| phn + 1 - phn| < 10 - 6. Benchmark validation was done by recreating the results of the analytical calculations (S = 0, no nanoparticles) with an error less than 2%.

Initially, spline expressions with fine-tuned parameters approximate the transformed equations. In the following, the obtained set of ODEs is utilized to generate a numerical dataset with the computational environment of Python-SciPy, along with the finite difference algorithm for velocity, temperature, and concentration of HNF $(MnZnFe_2O_4 + NiZnFe_2O_4 + H_2O)$ & simple NF $(MnZnFe_2O_4 + H_2O)$.

Following, the dataset is transformed and filtered in matrix form and sent to the MATLAB environment for neural component handling by AI techniques. The Levenberg–Marquardt Neural Network Algorithm (LMNA) is employed, which is exceptional for its self-learning mechanism. The performance of the algorithm is assessed on the test dataset, which again is organized into three subsets: training, testing, and validation. The load for these subsets is split into 70%, 15%, and 15%, respectively.

The Levenberg-Marquardt algorithm is an algorithm in nonlinear least-squares that is a combination of gradient descent and Gauss-Newton methods and allows the rapid convergence of nonlinear problems. Here, it has been driven by the relatively small size of the dataset as well as the requirement of high accuracy, where LMNN has performed better compared to the traditional backpropagation. This method is stable and fast at the same time, which is why it is very appropriate when considering complex transport processes in porous media.

The study examines eight conditions, including flow velocity, temperature, and concentration variation, and analyzes eight major influencing parameters. For the neural network model, an inner computation layer with 10 neurons and an output layer with 6 neurons is created. Analyses of three values for each parameter concerning the changes in both caloric and momentum across the modified wall boundaries are presented. Figure 3 depicts the data processing layout of the embedded data analysis system (created in MATLAB).

Parametric integrated values in the computational procedure are summarized in Table 3, and other extensive variables and coefficients are omitted through non-assumptions. Three versions of each variable are considered to analyze the overall trend of variation in HNF and NF.

Details of Training, Testing, and Validation (TTV) of the convergence parameter of LMNA for the various stages are listed in Table 4. It has a total of eight various situations accompanied by the MSE of TTV in columns 2–4 next to each of the situations. In columns 5–7, original output performance and slopes of landscape and step

Fig. 3. Diagram of the Levenberg-Marquardt neural network algorithm (LMNA).

		Parameters							
Scenarios	Cases	В	r	Fr	Ec	Pr	Sc	E	K
S-1	1	0.2	0.3	0.2	0.2	2.0	0.8	0.2	0.2
Variation of	2	0.6	0.3	0.2	0.2	2.0	0.8	0.2	0.2
$B \text{ for } f'(\eta) \text{ profile}$	3	1.0	0.3	0.2	0.2	2.0	0.8	0.2	0.2
S-2	1	0.3	0.2	0.2	0.2	2.0	0.8	0.2	0.2
Variation of	2	0.3	0.6	0.2	0.2	2.0	0.8	0.2	0.2
r for $f'(\eta)$ profile	3	0.3	1.0	0.2	0.2	2.0	0.8	0.2	0.2
S-3	1	0.3	0.2	0.2	0.2	2.0	0.8	0.2	0.2
Variation of	2	0.3	0.2	0.6	0.2	2.0	0.8	0.2	0.2
$Fr \text{ for } f'(\eta) \text{ profile}$	3	0.3	0.2	1.0	0.2	2.0	0.8	0.2	0.2
S-4	1	0.3	0.2	0.2	0.0	2.0	0.8	0.2	0.2
Variation of	2	0.3	0.2	0.2	0.5	2.0	0.8	0.2	0.2
$Ec \text{ for } \theta(\eta) \text{ profile}$	3	0.3	0.2	0.2	1.0	2.0	0.8	0.2	0.2
S-5	1	0.3	0.2	0.2	0.3	0.1	0.8	0.2	0.2
Variation of	2	0.3	0.2	0.2	0.3	0.6	0.8	0.2	0.2
$Pr \text{ for } \theta(\eta) \text{ profile}$	3	0.3	0.2	0.2	0.3	1.0	0.8	0.2	0.2
S-6	1	0.1	0.1	0.1	0.1	0.1	0.1	0.1	0.01
Variation of	2	0.1	0.1	0.1	0.1	0.1	0.2	0.1	0.01
$Sc \text{ for } \varphi(\eta) \text{ profile}$	3	0.1	0.1	0.1	0.1	0.1	0.3	0.1	0.01
S-7	1	0.5	0.9	0.3	0.3	1.6	1.3	0.1	0.1
Variation of	2	0.5	0.9	0.3	0.3	1.6	1.3	0.6	0.1
$E \text{ for } \varphi (\eta) \text{ profile}$	3	0.5	0.9	0.3	0.3	1.6	1.3	1.0	0.1
S-8	1	0.9	0.2	0.3	0.3	1.6	0.9	0.5	0.01
Variation of	2	0.9	0.2	0.3	0.3	1.6	0.9	0.5	0.06
$k \text{ for } \varphi(\eta) \text{ profile}$	3	0.9	0.2	0.3	0.3	1.6	0.9	0.5	0.10

Table 3. Numerical Scenarios of Darcy Forchheimer flow for several studied cases. Significant values are in bold.

size grids are shown. Further, the number of iterations is presented in the penultimate column, while the last column lists the duration of the iterations.

Table 5 shows the MSE of TTV ranges up to 10^{-11} and agrees with other grid parameters. Computational units are designed to process at the highest level of succinctness and precision. The visualization and graphs of tabulated data are presented in the next section.

Even though LMNN networks are sensitive to overfitting in case of over-parameterization, in the current work, the risk was reduced through limiting the number of hidden neurons, cross-validation, and tracking validation errors. The fact that training and testing profile closely matched each other proves that the model was applicable to unseen data.

The flow chart in Fig. 4 provides an overview of all stages in the computational procedure of the problem, which are illustrated with different blocks. Starting from PDEs to final AI-based comparison outputs and error plots.

Results and discussion

The graphical visualization of TTV of the AI algorithm holds fitness curves, MSE histograms, regression analysis, performance, and training plots. A comparison of two competing fluids against thermophysical influences is produced and made available for enhanced visualization, enabling a perfect understanding of the reason for choosing HNF instead of NF. Numerical validation of the results is done by dropping all influences (set to 0) except Pr and Sc as 0.1 (Table 5).

Figure 5, 6, 7, 8 and 9 illustrates the LMNA-TTV profiles programmed by the MATLAB environment. These diagrams are generated around target Python-gen data, capturing the errors in AI-gen outputs.

	MSE data							
Scenario	Training	Validation	Testing	Performance grids	Gradient grids	Mu grids	Closing epoch	T/sec
S-1	1.76×10 ⁻¹⁰	2.26×10 ⁻¹⁰	1.44×10 ⁻¹⁰	1.76×10 ⁻¹⁰	9.96×10 ⁻⁰⁸	1.00×10 ⁻⁰⁸	302	01
S-2	3.99×10 ⁻¹⁰	6.89×10 ⁻¹⁰	5.18×10 ⁻¹⁰	3.99×10 ⁻¹⁰	9.96×10 ⁻⁰⁸	1.00×10 ⁻⁰⁸	280	01
S-3	5.59×10 ⁻¹¹	7.60×10 ⁻¹¹	8.04×10 ⁻¹¹	5.59×10 ⁻¹¹	9.99×10 ⁻⁰⁸	1.00×10 ⁻⁰⁹	707	03
S-4	6.60×10 ⁻¹⁰	9.34×10 ⁻¹⁰	9.16×10 ⁻¹⁰	6.60×10 ⁻¹⁰	9.96×10 ⁻⁰⁸	1.00×10 ⁻⁰⁸	252	01
S-5	1.26×10 ⁻⁰⁹	3.50×10 ⁻⁰⁹	1.90×10 ⁻⁰⁹	1.26×10 ⁻⁰⁹	9.95×10 ⁻⁰⁸	1.00×10 ⁻⁰⁸	503	02
S-6	4.82×10 ⁻¹⁰	8.42×10 ⁻¹⁰	9.36×10 ⁻¹⁰	4.82×10 ⁻¹⁰	9.82×10 ⁻⁰⁸	1.00×10 ⁻¹⁰	404	01
S-7	1.79×10 ⁻⁰⁹	2.18×10 ⁻⁰⁹	2.62×10 ⁻⁰⁹	1.79×10 ⁻⁰⁹	9.94×10 ⁻⁰⁸	1.00×10 ⁻⁰⁸	522	02
S-8	2.43×10 ⁻¹⁰	3.11×10 ⁻¹⁰	5.19×10 ⁻¹⁰	2.43×10 ⁻¹⁰	9.99×10 ⁻⁰⁸	1.00×10 ⁻⁰⁹	144	01

Table 4. Convergence parameters for dataset.

Fr	σ_1 (%)	σ_2	Python-generated $f'(0)$	AI-generated $f'(0)$	Absolute error
0.1	5	Nil	1.4213395	1.4213113	0.0000282
0.2	5	Nil	1.3942365	1.3942208	0.0000157
0.3	5	Nil	1.3690062	1.3690011	0.0000051
0.1	5	5%	1.3163499	1.3163467	0.0000032
0.2	5	5%	1.2912994	1.2913070	0.0000076
0.3	5	5%	1.2679778	1.2679945	0.0000167

Table 5. Validation of results for initiating velocity.

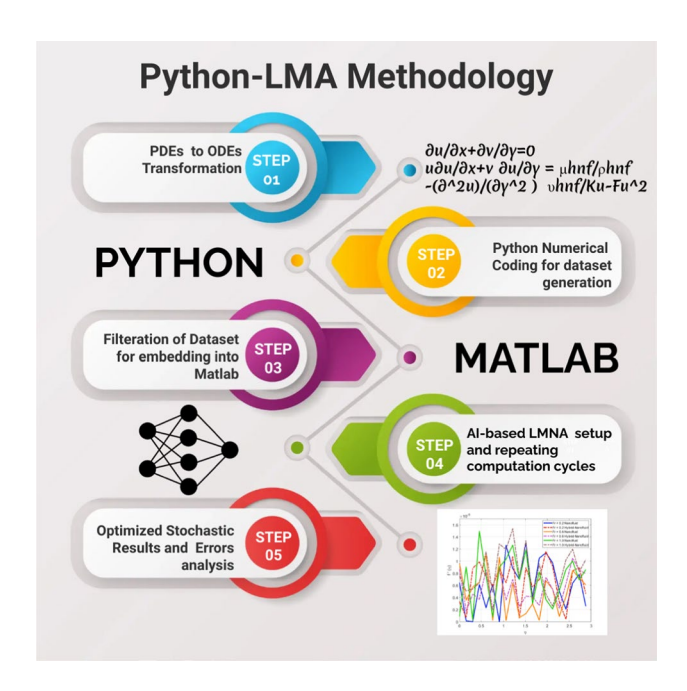


Fig. 4. Flow chart of problem evaluation and solving procedure.

In any case, Fig. 5 illustrates the three curves of TTV—Training (blue), Validation (green), and Testing (red) overlays. The dotted line presents the best fit, starting from zero epoch to the maximum. The graphs of both input and output variables in parallel curves stand for the actual change and are more apparent for the best values. The number of the largest epoch is 707 for the validation of 10^{-11} . All the curves follow the same trajectory and crusts and troughs of the dataset; thus, it confirms the computation of the neural network.

MSE oscillations in Fig. 5 occur at small x values based on the model's fine-tuning phases, in which the parameters and weights are being adapted. This is quite unexpected since the learning rate first induces fluctuations and then produces a stable MSE. Moreover, when we have numerous parameters interrelating in the AI-based approach, this might first complicate error sensitivity in the rate. These oscillations decrease as

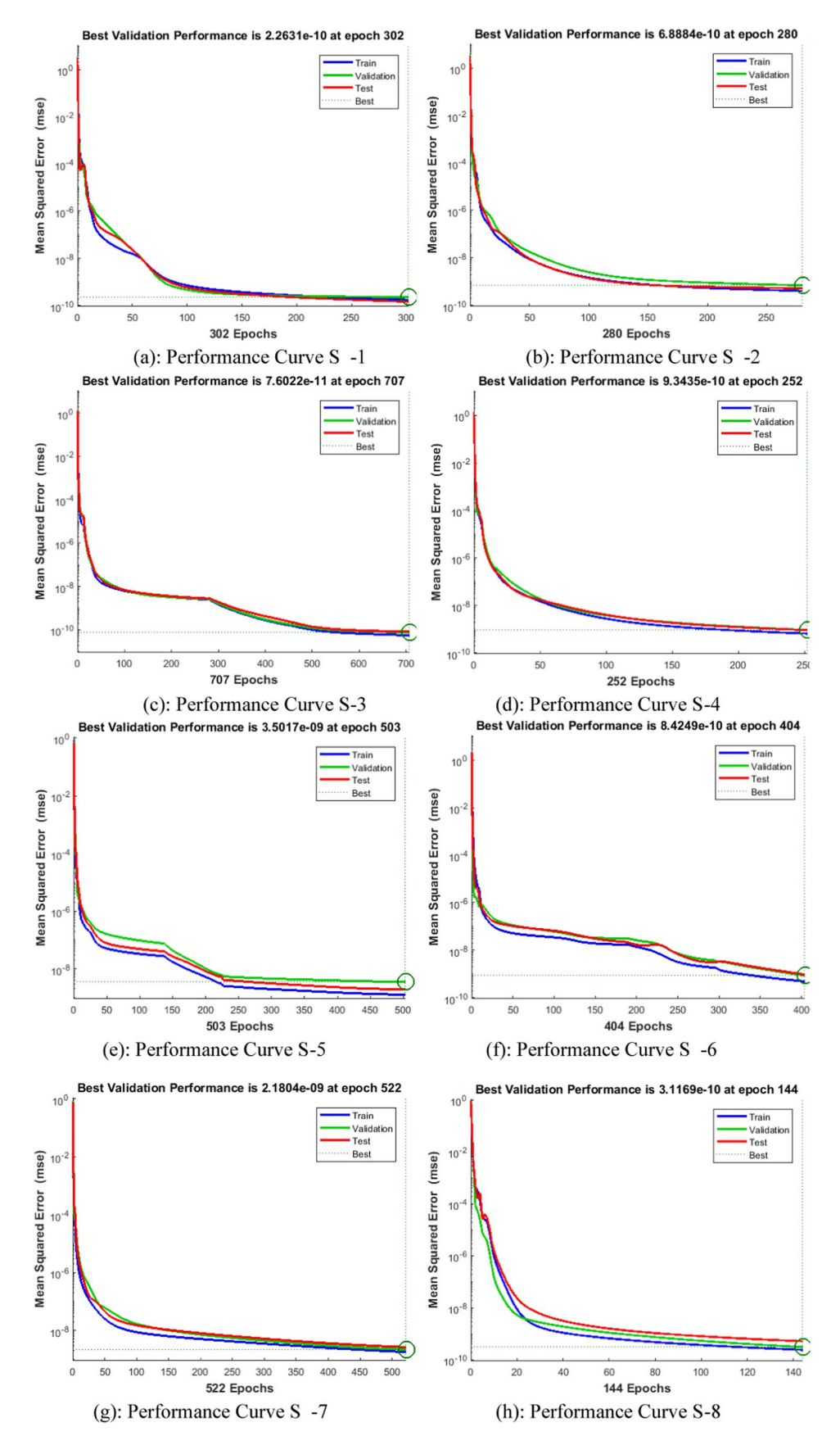


Fig. 5. TTV performance profile of LMNA.

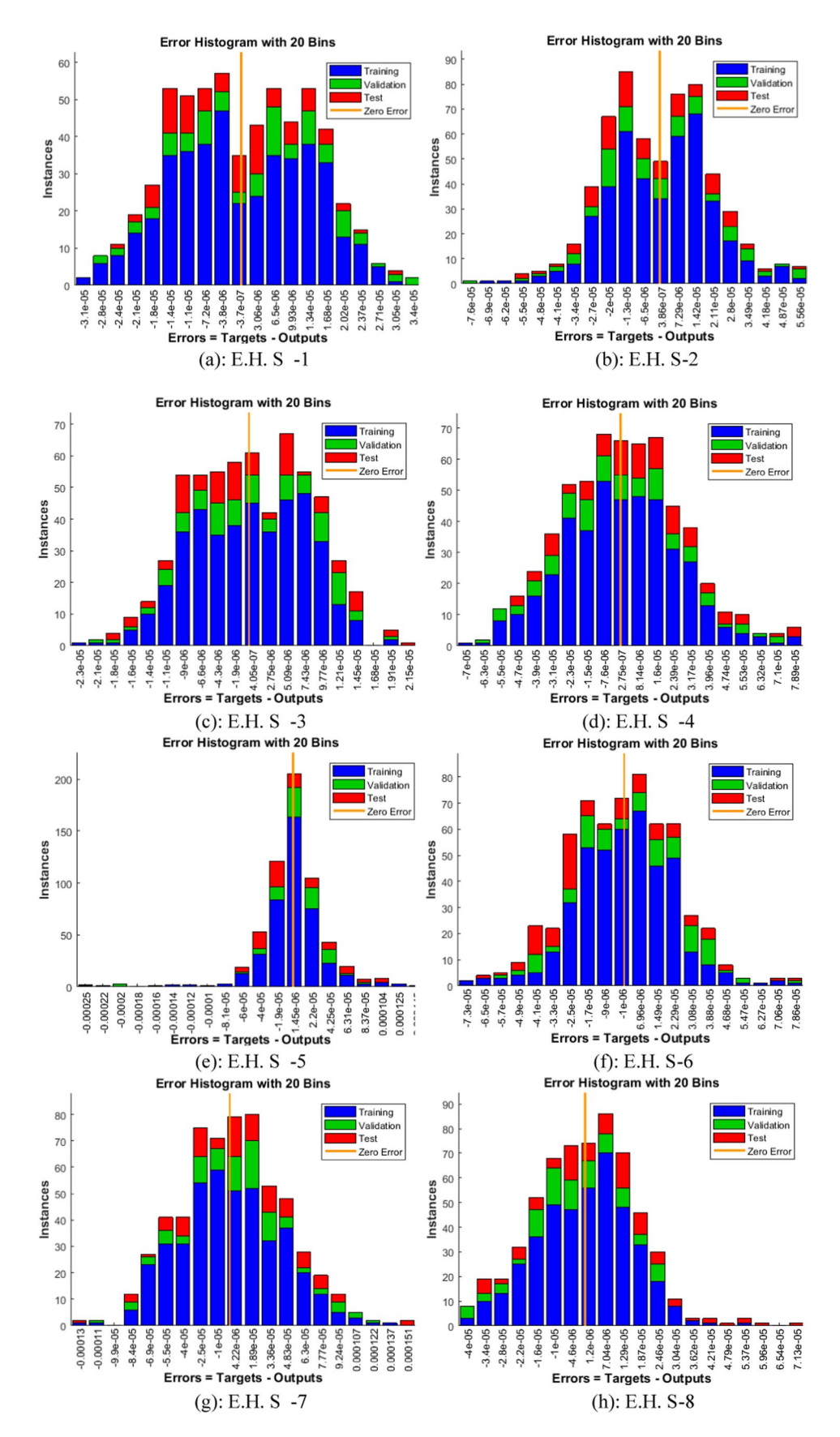


Fig. 6. TTV error histograms (E.H.) Profile of LMNA.

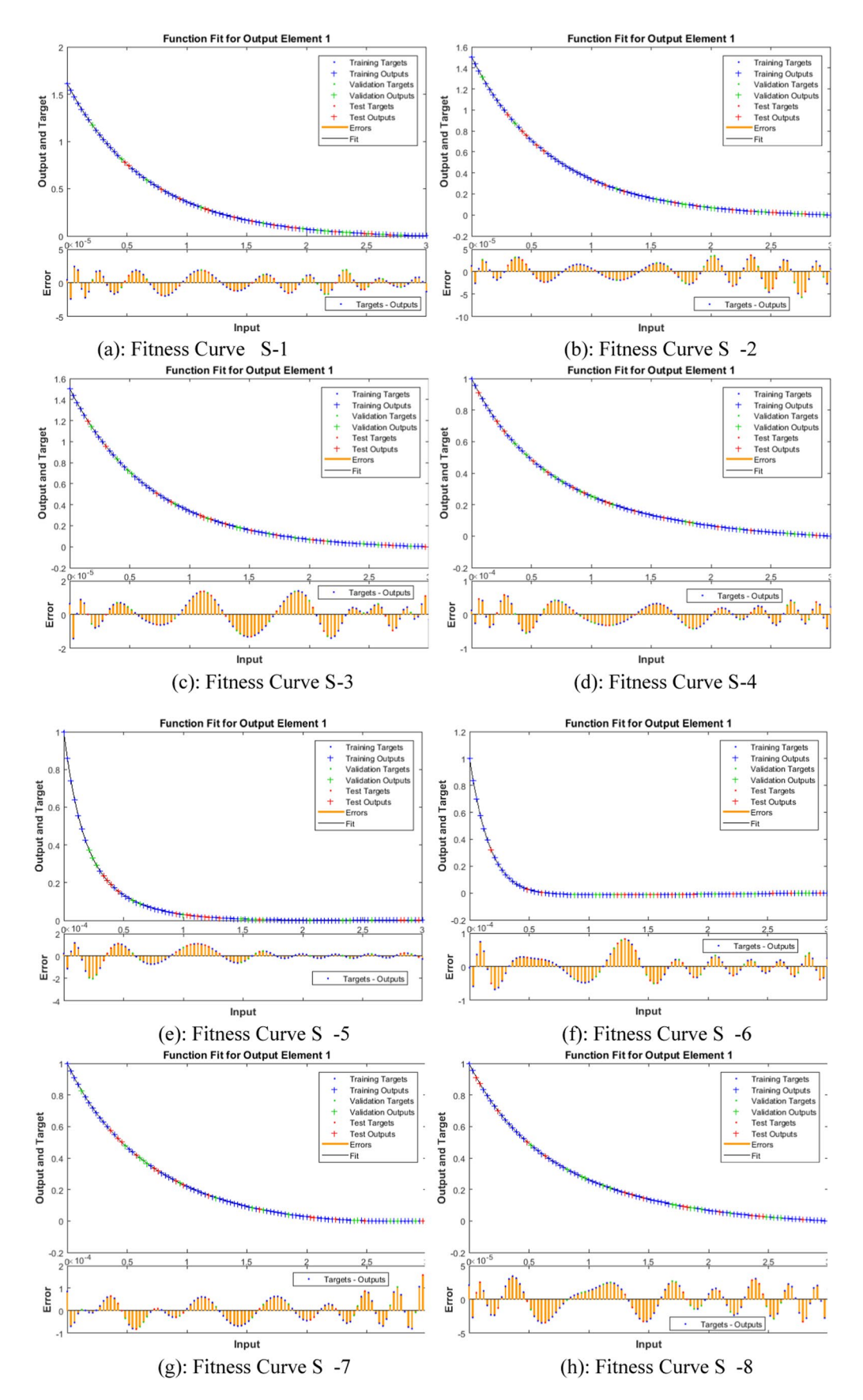


Fig. 7. TTV Fitness Profile of LMNA.

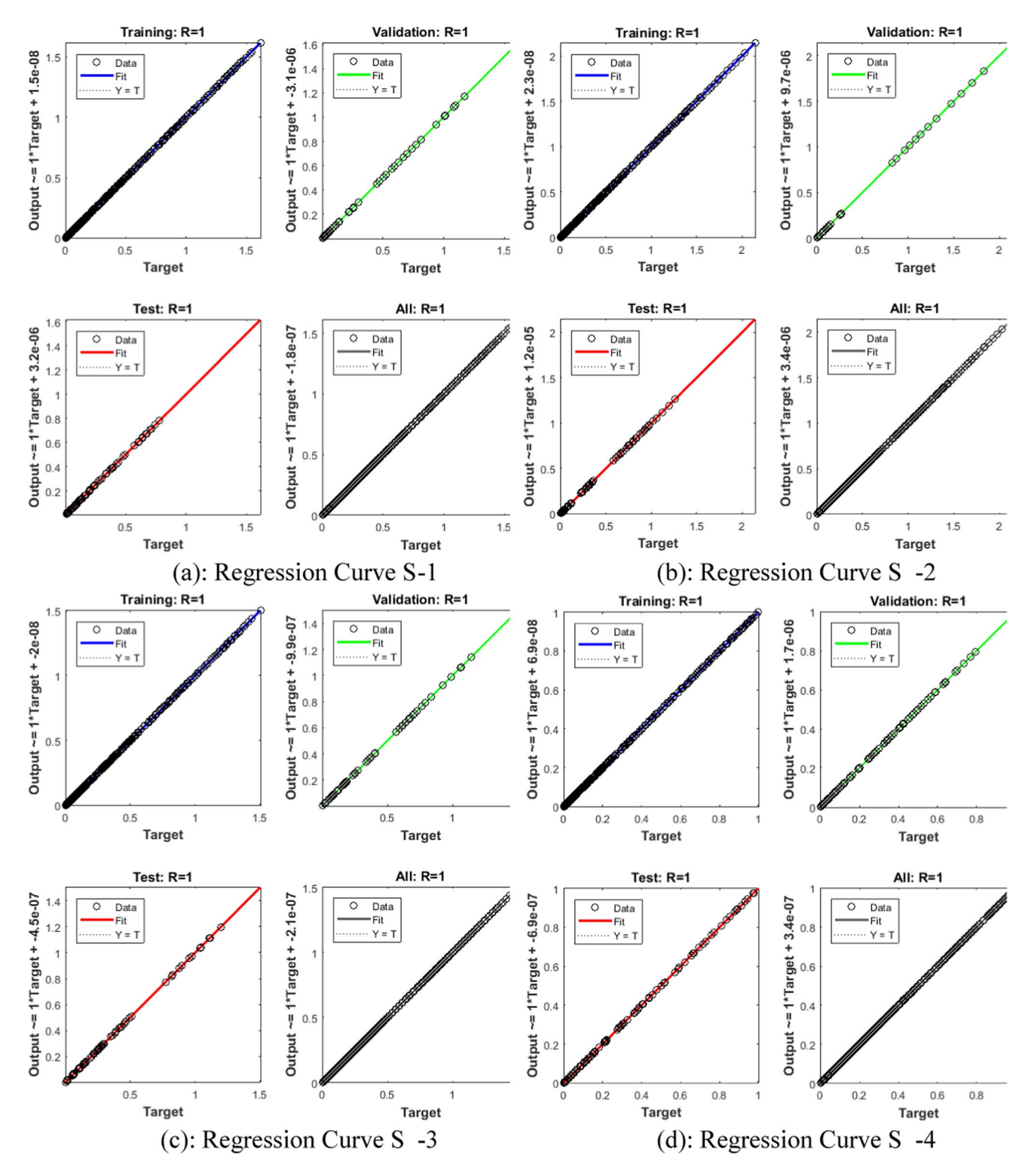


Fig. 8. Regression analyses profile of LMNA.

learning proceeds and become more similar across time as training continues, though of course, they are still more pronounced in earlier phases of learning.

Figure 6 provides the respective Mean Squared Error (MSE) histograms related to the Training–Testing-Validation (TTV) performance profile as Fig. 5 above. The histogram is a chart illustrating the distribution of errors in each set of data i.e., training (blue), validation (green), and testing (red), with the yellow line running upwards indicating the point of zero error. The dataset generated by Python has been divided into 20 equal bins, where the TTV practices are well indicated in the bars. The plots on the horizontal axis represent the difference between the target and the predicted output, and the vertical axis represents the frequency of the occurrence at a

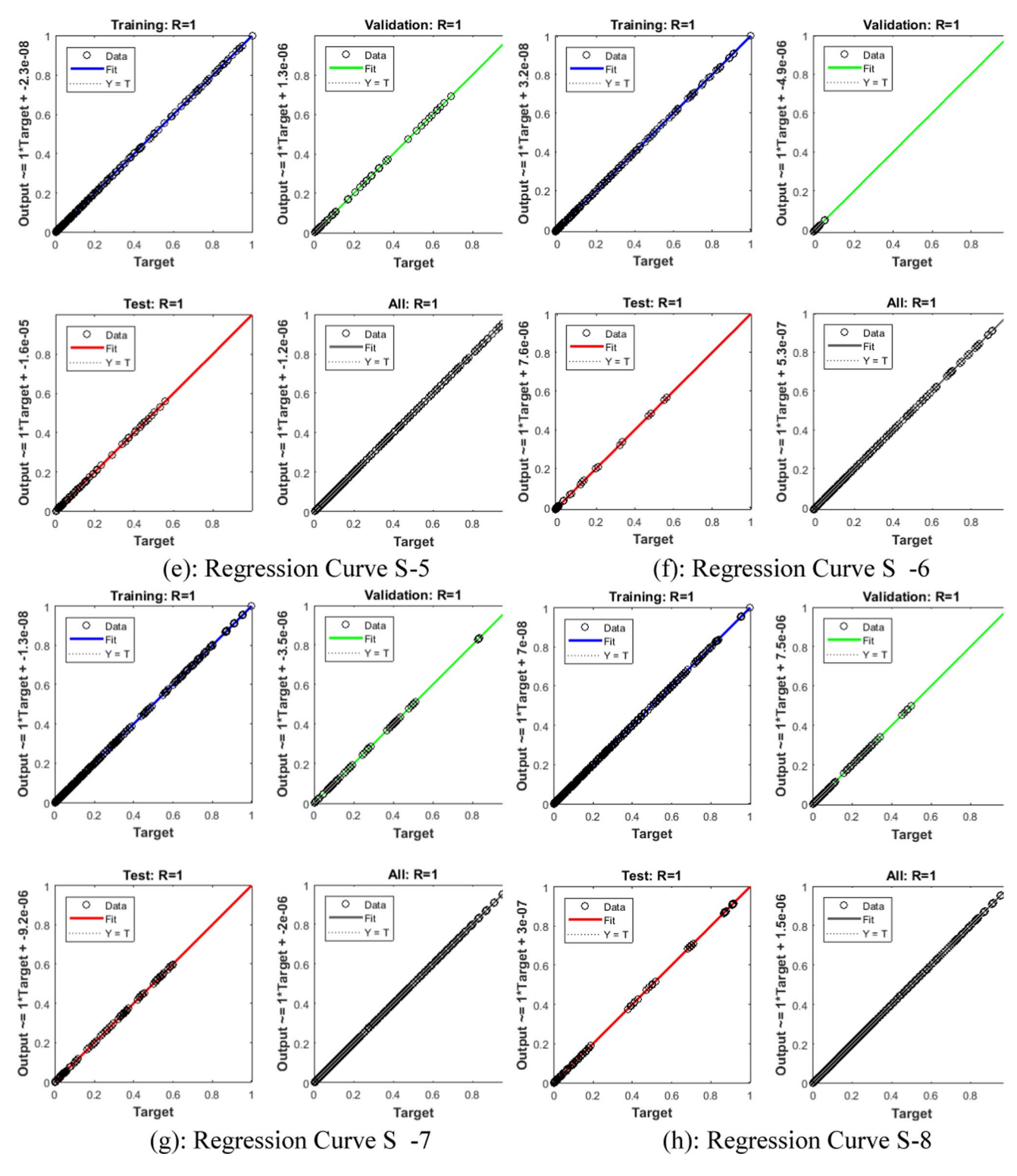


Fig. 8. (continued)

certain magnitude of error. It is possible to visually compare the distribution of errors on the various partitions of the dataset using this visualization, which ensures that the LMNN model is free of overfitting since the training, validation, and testing errors are tightly clustered around the zero-error line.

The fitness profile of the Levenberg-Marquardt Neural Algorithm (LMNA) and the error profile are presented in Fig. 7. The crosses that were marked in the legend represent the various partitions of the dataset (training, validation, and testing), which all have a similar trajectory. The consistency indicates that a good fit of the LMNA has been attained, and it will approximate the numerical solution. The error curve presents slight oscillations, as it should be, since the weights and biases adjust during training. These small variations also aid in

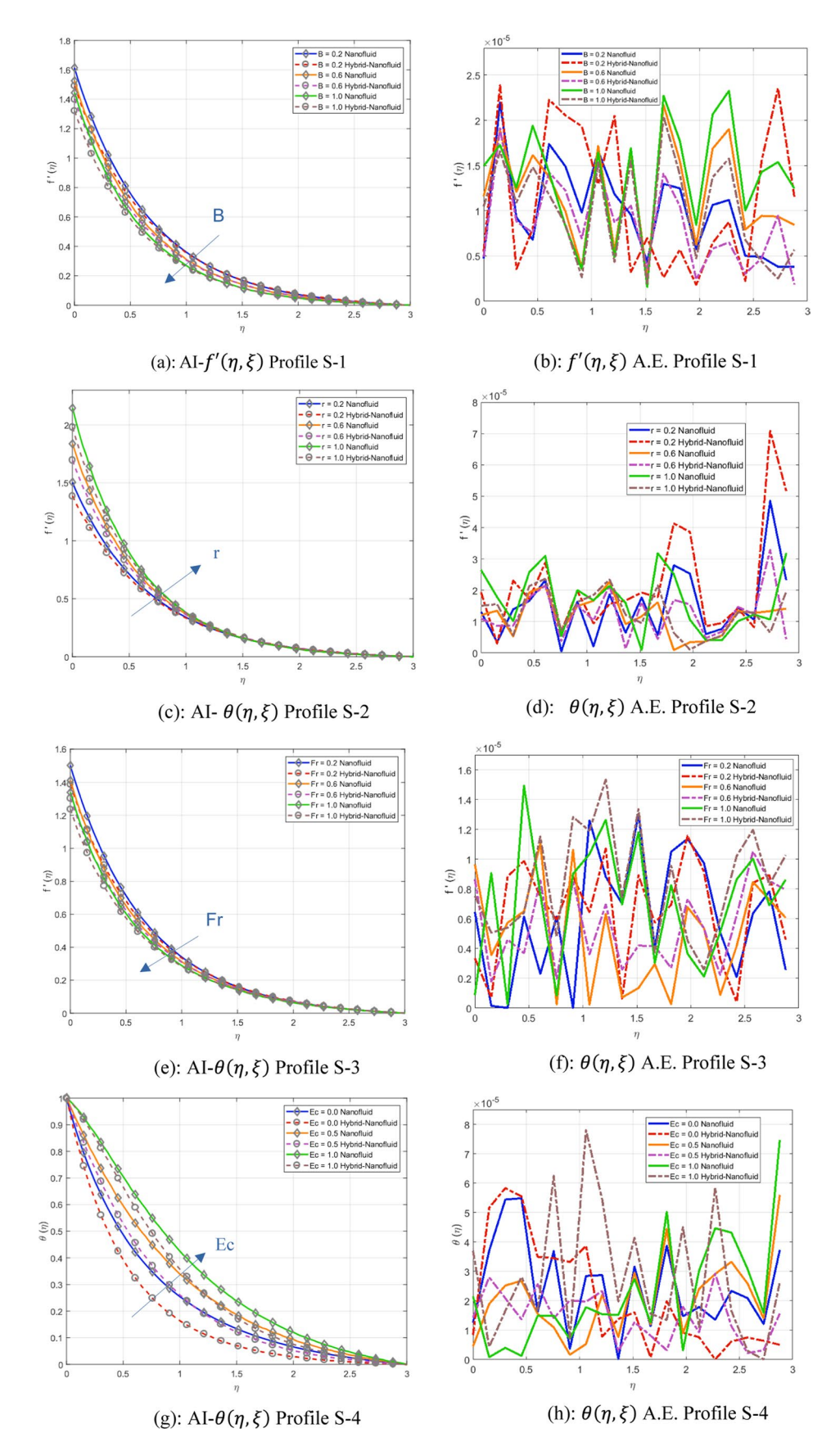


Fig. 9. AI-based LMNA Solutions and Absolute-Errors (A.E.) of HNF vs NF.

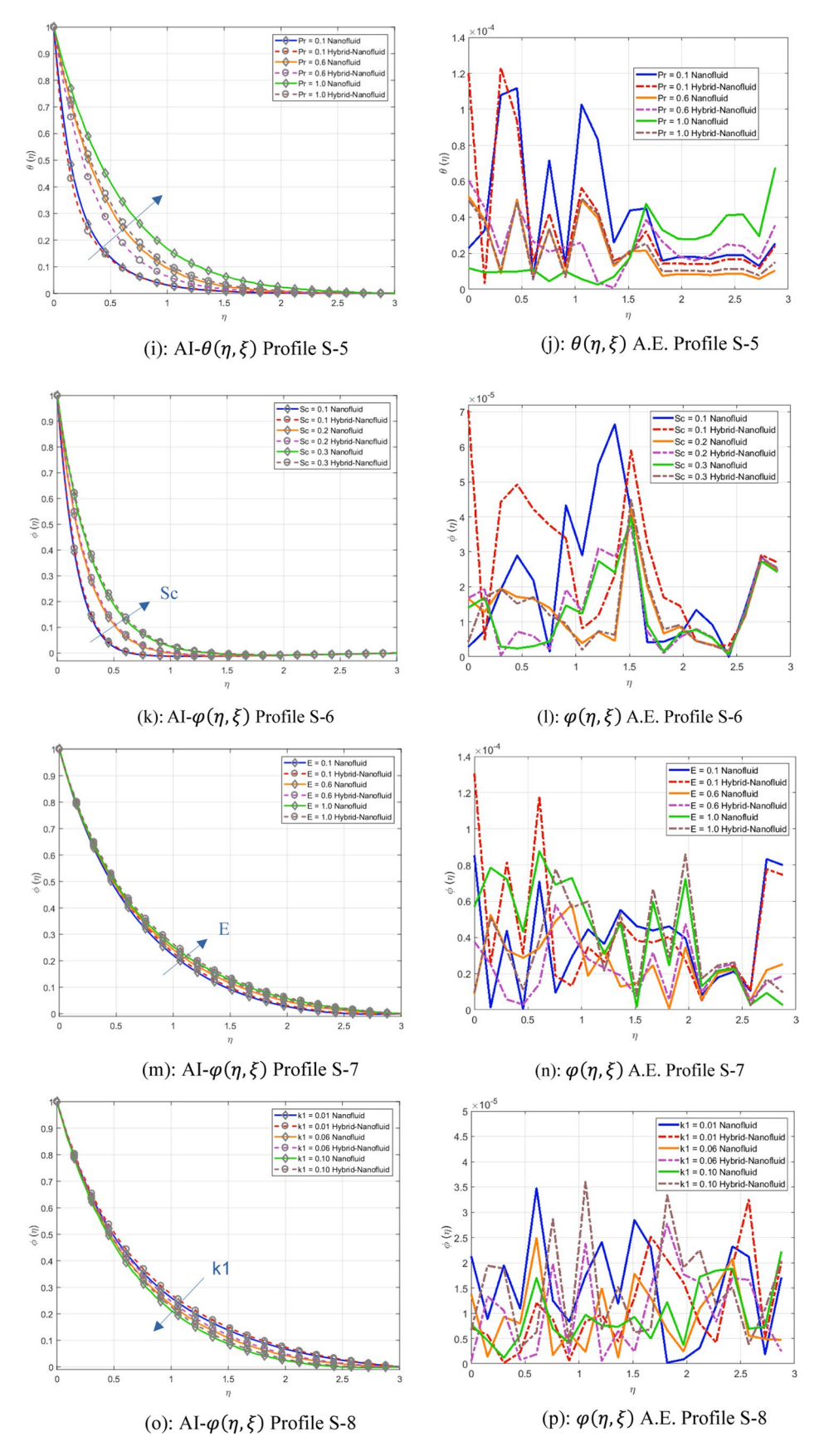


Fig. 9. (continued)

making the model not too rigid and thus, it is possible to generate smooth outputs without necessarily losing the generalization ability. Controlled randomness being part of the training process therefore, leads to the strength and stability of the predicted results.

Figure 8 presents nomograms of TTV. In all the graphs of regression, the gradient of the line is equal to the unit, which means the target is proportional to the output. In this case, regression slopes are best fit by convergence. The plot for each dataset of training, testing, and validation is proven for each scenario. Moreover, an average of all three TTV datasets is added with a black output gradient.

Along with MSE and regression plots, R2 values (0.995–0.999), residual histogram, and predictions versus reference value scatter plot are shown (Figs. 6 and 8). The relative errors $(10^{-3}-10^{-4})$ are less than 1 percent of the Nusselt and Sherwood numbers, which is sufficiently insignificant to allow for the engineering analysis of microchannel heat exchangers and porous media reactors. In this manner, LMNN predictions can be considered statistically and physically valid.

Finally, Fig. 9 presents the AI-generated solutions and their absolute differences in numerical outcomes. Subfigure 9a, c, e stands for AI-generated velocities of HNF with dashed and NF with solid lines. Both the nanofluids exhibit the same pattern, and the difference between velocities is wider at the start, which decreases to zero with increasing time. The velocity profile is wider due to a strong surface tension gradient, starting thermal difference, and interaction of nanoparticles within the boundary layer. As the effects diminish due to thermal diffusion, thermocapillary forces, and stabilizing particle interaction, leading to monotonous convergence.

Subfigure 9g, i is the temperature profile. These curves are close at the start due to homogeneous boundary conditions. With the increase in the curves separated apart due to differing thermal properties and the significant impacts of Ec and Pr near the boundary layer. These parameters affect the rate of viscous dissipation, thermal diffusion, and mass transfer, causing divergence and system approaches to thermal equilibrium.

The following subfigures 9k, m, o present a concentration profile that starts with all curves together due to homogeneous boundary conditions. It gets wider as the values influencing parameters increase with the rise in concentration and reaches mass transfer equilibria with concentration stabilization.

The hybrid system has a better effective thermal conductivity and greater thermocapillary forces than the conventional nanofluids. This is in line with the effective medium theory, in which the availability of ferrite nanoparticles creates some extra heat conduction routes and alters the interfacial tension. This recorded improvement in the Nusselt and Sherwood numbers is therefore indicative of a combined effect of both the MnZnFe2O4 and NiZnFe2O4 particles, other than the individual nanofluids can produce.

Compared with the base fluid, the heat transfer behavior of the hybrid nanofluid is controlled by several parameters, including the Darcy and Forchheimer numbers, the Marangoni ratio, the Eckert number, and the Prandtl number. For example, an augmentation of the Darcy number leads to a reduction of the fluid's velocity so that convective heat transfer and thermal diffusion in the porous material are restricted. This restriction is still in contrast with the effect of the Marangoni ratio, which stimulates surface-driven convection and heat transfer through temperature gradients. The presence of MnZnFe₂O₄ & NiZnFe₂O₄ nanoparticles in the base fluid enhances the thermal conductivity compared to a single-phase nanofluid, as shown by T-H curves. Such properties show that hybrid nanofluids can improve thermal applications in microelectronics and renewable energy systems through the ability to sustain temperature gradients and heat flow rates in all flow rates. These findings can be used as the basis for future research on ways to figure out the right concentrations of components to incorporate in hybrid nanofluids to boost thermal performance, for various engineering uses.

Sensitivity analysis was done based on perturbing the input parameters (Pr, Ec, Da, Fr) about $\pm 5\%$. The LMNN results were within 2 percent of each other, which validates the strength. Also, a Monte Carlo simulation of 500 random samples of input ranges was conducted, and the average prediction error was less than 1%. These findings indicate that the LMNN model is stable in uncertainty in mixture nanofluid properties.

The higher the Darcy number, the lower the flow resistance, and this increases velocity at the expense of temperature gradients because of quicker convective transport. Conversely, an increase in Forchheimer numbers brings on the inertial drag that decreases velocity. The thermocapillary forces present due to the gradient of surface tension cause the fluid to move toward the surface with increased velocity, which increases the rate of Marangoni convection. Eckert number increases fluid temperature because of viscous dissipation, and the Prandtl number determines the relative thickness of the momentum and thermal boundary layers.

The model can be used in microchannel cooling systems, porous reactors, and in surface-tension-driven flows in materials processing. Yet, the cost of the LMNN training on large datasets is the practical constraint, as well as sensitivity to the noisy data, which should be addressed in future studies. Though this may require the computationally intensive LMNN on large-scale data, in our case the training set was not large, and the algorithm converged within several seconds. In the case of bigger systems, parallelization or other optimizers can be needed. However, the precision and fast convergence that LMNN provides it suitable in mid-scale engineering tasks where precision is more important compared to real-time specifications.

Conclusion

This numerical study delves into a machine learning-based comparative analysis of Marangoni convection involving a simple hybrid nanofluid, specifically $MnZnFe_2O_4$ and $NiZnFe_2O_4$ in a water base (H_2O) . The numerical data is gathered using a Python-based finite difference algorithm, with subsequent AI-driven analysis performed within the MATLAB environment. Key parameters influencing thermal dissipation are assessed, including heat transfer, mass transfer, and the irreversibility of viscous dissipation within the flow. The principal findings are summarized as follows:

- Both HNF and NF experience a decrease in flux as the inverse Darcy-Forchheimer value rises (Fig. 9a), with a more pronounced decrease observed in HNF compared to NF. This sudden drop is due to the addition of a second nano-solute.
- The flow rate's increase with a higher Marangoni ratio is less prominent in HNF than in NF (Fig. 9c).
- The velocity reduction as the Forchheimer number increases is more significant in HNF than in NF (Fig. 9e).
- An increased Eckert number enhances viscous dissipation, thereby raising the temperature profile near the boundary, with this increase being more gradual in NF than in HNF (Fig. 9g, i).
- A rise in both Schmidt value and activation energy results in a higher concentration profile, having a slightly greater impact in HNF than in NF (Fig. 9(k, m)).
- Concentration decreases with a higher chemical reaction rate, with corresponding values being greater for HNF as opposed to NF (Fig. 90).
- The absolute error values validate the AI results, with AI-generated outputs to the numerical dataset in Fig. 9 (b, d, f, h, j, l, n, p) being significantly different from zero.

This article presents a new approach to predicting and controlling Marangoni convection in hybrid nanofluids using machine learning (ML) techniques. The research highlighted the role of crucial parameters like the Darcy and Forchheimer numbers, Eckert ratio, and Prandtl number in governing convective heat transfer and overall fluid dynamics in hybrid nanofluids as opposed to standard nanofluids. Our findings indicate that the Levenberg–Marquardt neural network in Artificial Intelligence achieved greater accuracy than traditional deterministic model benchmarks, offering a groundbreaking method for fluid dynamic calculations.

This paper demonstrates that LMNN provides accurate forecasts of Marangoni convection in hybrid nanofluids for Darcy-Forchheimer porous media. Some of the critical results are the justification of LMNN investigations with literature and with parameter alterations and data sets. The method has potential extensions to other hybrid nanofluids, non-uniform geometries, and real-time predictive computational modeling, both in energy and biomedical engineering applications.

Thus, the prospects for advancing hybrid nanofluids in complex heat transfer systems across industrial, biomedical, and environmental engineering fields are promising. Therefore, the proposed AI framework can serve as a foundation for creating real-time predictive models that aim to regulate temperature in engineering practices, while also enhancing the understanding of thermal optimization techniques across various engineering disciplines. Ultimately, this paper lays the groundwork for the development of innovative AI-driven thermodynamic applications and investigates novel applications of nanofluids to enhance heat transfer systems.

Data availability

The authors confirm that the data that supports the findings of this study are available within the article. Raw data that support the finding of this study are available from the corresponding author, upon reasonable request.

Received: 11 August 2025; Accepted: 6 October 2025

Published online: 12 November 2025

References

- 1. Mahdi, R. A., Mohammed, H. A., Munisamy, K. M. & Saeid, N. H. Review of convection heat transfer and fluid flow in porous media with nanofluid. *Renew. Sustain. Energy Rev.* 41, 715–734 (2015).
- 2. Sankar, M., Swamy, H. A. K., Do, Y. & Altmeyer, S. Thermal effects of nonuniform heating in a nanofluid filled annulus: Buoyant transport versus entropy generation. *Heat Transf* https://doi.org/10.1002/htj.22342 (2021).
- 3. Abbas, M. et al. Numerically analysis of Marangoni convective flow of hybrid nanofluid over an infinite disk with thermophoresis particle deposition. *Sci. Rep.* 13, 5036. https://doi.org/10.1038/s41598-023-32011-x (2023).
- 4. Rosensweig, R. E. Ferrohydrodynamics (Cambridge University Press, 1985).
- 5. Altmeyer, S. Ferrofluids. Scholarpedia 15(11), 55163 (2020).
- 6. http://www.scholarpedia.org/article/Ferrofluids.
- 7. Gowda, P., Sankar, M., Salah, A. & Altmeyer, S. A. Buoyant flow and thermal analysis in a nanofluid-filled cylindrical porous annulus with a circular baffle: A computational and machine learning-based approach. *Mathematics* 13, 2027 (2025).
- 8. Buongiorno, J. Convective transport in nanofluids (2006).
- 9. Kshirsagar, D. P. & Venkatesh, M. A. A review on hybrid nanofluids for engineering applications. *Mater. Today: Proc.* 44, 744–755 (2021).
- Ahmad, B., Abbas, T., Fatima, K., Duraihem, F. Z. & Saleem, S. Nonlinear flow of hybrid nanofluid with thermal radiation: A numerical investigation. ZAMM-J. Appl. Math. Mech./Zeitschrift für Angewandte Mathematik und Mechanik 104(1), e202200170 (2024).
- 11. Buongiorno, J. and Hu, L.W., 8. Innovative Technologies: Two-Phase heat transfer in Water-Based nanofluids for nuclear applications final report (No. DOE/ID/14765-8). Massachusetts Institute of Technology Cambridge, MA 02139-4307 2009.
- 12. Tiwari, R. K. & Das, M. K. Heat transfer augmentation in a two-sided lid-driven differentially heated square cavity utilizing nanofluids. *Int. J. Heat Mass Transf.* 50(9–10), 2002–2018 (2007).
- 13. Pordanjani, A. H. et al. Nanofluids: Physical phenomena, applications in thermal systems and the environment effects-a critical review. *J. Clean. Prod.* 320, 128573 (2021).
- 14. Liu, Z. et al. Numerical bio-convective assessment for rate type nanofluid influenced by Nield thermal constraints and distinct slip features. Case Stud. Therm. Eng. 44, 102821 (2023).
- Soudagar, M. E. M. et al. Optimizing IC engine efficiency: A comprehensive review on biodiesel, nanofluid, and the role of artificial intelligence and machine learning. *Energy Convers. Manag.* 307, 118337 (2024).
- Wang, X. et al. Nanofluids application in machining: A comprehensive review. Int. J. Adv. Manuf. Technol. 131(5), 3113–3164 (2024).
- Sheikholeslami, M. & Khalili, Z. Simulation for impact of nanofluid spectral splitter on efficiency of concentrated solar photovoltaic thermal system. Sustain. Cities Soc. 101, 105139 (2024).
- Bani-Fwaz, M. Z. et al. Computational investigation of thermal process in radiated nanofluid modulation influenced by nanoparticles (Al₂O₃) and molecular (H₂O) diameters. J. Comput. Des. Eng. 11(2), 22–36 (2024).
- 19. Wang, J. et al. A review on nanofluid stability: Preparation and application. Renew. Sustain. Energy Rev. 188, 113854 (2023).

- Alsabery, A. I. et al. Convection heat transfer in enclosures with inner bodies: A review on single and two-phase nanofluid models. Renew. Sustain. Energy Rev. 183, 113424 (2023).
- Khan, M. & Khan, W. A. Steady flow of Burgers' nanofluid over a stretching surface with heat generation/absorption. J. Braz. Soc. Mech. Sci. Eng. 38(8), 2359–2367 (2016).
- 22. Modi, K. V., Patel, P. R. & Patel, S. K. Applicability of mono-nanofluid and hybrid-nanofluid as a technique to improve the performance of solar still: A critical review. *J. Clean. Prod.* 387, 135875 (2023).
- 23. Li, S. et al. Analysis of the Thomson and Troian velocity slip for the flow of ternary nanofluid past a stretching sheet. Sci. Rep. 13(1), 2340 (2023).
- 24. Ahmad, S. & Nadeem, S. Thermal analysis in buoyancy driven flow of hybrid nanofluid subject to thermal radiation. *Int. J. Ambient Energy* **43**(1), 3868–3876 (2020).
- 25. Sreenivasulu, M. B. & Vijaya, R. Influence of activation energy on the hybrid nanofluid flow over a flat plate with quadratic thermal radiation: An irreversibility analysis. *Int. J. Ambient Energy* **43**(1), 8878–8887 (2022).
- 26. Sushma, S., Pavithra, C.G., Gowtham, K.J. and Gireesha, B.J., Impact of similarity transformations on hybrid nanofluid thermal behavior with thermal radiation on nonlinear stretching surface via Hermite wavelet transformations. *Radiat. Eff. Defects Solids*, pp.1–25 2024.
- 27. Li, Y. X. et al. Numerical treatment of time dependent magnetohydrodynamic nanofluid flow of mass and heat transport subject to chemical reaction and heat source. Alex. Eng. J. 61(3), 2484–2491 (2022).
- 28. Awan, S. E., Raja, M. A. Z., Mehmood, A., Niazi, S. A. & Siddiqa, S. Numerical treatments to analyze the nonlinear radiative heat transfer in MHD nanofluid flow with solar energy. *Arab. J. Sci. Eng.* **45**, 4975–4994 (2020).
- Prakash, J., Tripathi, D. & Bég, O. A. Computation of EMHD ternary hybrid non-Newtonian nanofluid over a wedge embedded in a Darcy-Forchheimer porous medium with zeta potential and wall suction/injection effects. *Int. J. Ambient Energy* 44(1), 2155– 2169 (2023).
- 30. Ellahi, R., Tariq, M. H., Hassan, M. & Vafai, K. On boundary layer nano-ferroliquid flow under the influence of low oscillating stretchable rotating disk. *J. Mol. Liq.* 229, 339–345 (2017).
- 31. Jamshed, W. et al. Numerical simulations of environmental energy features in solar pump applications by using hybrid nanofluid flow: Prandtl-Eyring case. *Energy Environ.* **34**(4), 780–807 (2023).
- 32. Chakraborty, S. & Panigrahi, P. K. Stability of nanofluid: A review. Appl. Therm. Eng. 174, 115259 (2020).
- 33. Muneeshwaran, M., Srinivasan, G., Muthukumar, P. & Wang, C. C. Role of hybrid-nanofluid in heat transfer enhancement-A review. *Int. Commun. Heat Mass Transf.* 125, 105341 (2021).
- Sarkar, J., Ghosh, P. & Adil, A. A review on hybrid nanofluids: Recent research, development, and applications. Renew. Sustain. Energy Rev. 43, 164–177 (2015).
- 35. Qureshi, M. A. Thermal capability and entropy optimization for Prandtl-Eyring hybrid nanofluid flow in solar aircraft implementation. *Alex. Eng. J.* 61(7), 5295–5307 (2022).
- 36. Shah, Z., Rooman, M. & Shutaywi, M. Computational analysis of radiative engine oil-based Prandtl-Eyring hybrid nanofluid flow with variable heat transfer using the Cattaneo-Christov heat flux model. RSC Adv. 13(6), 3552–3560 (2023).
- 37. Shehzad, S. A., Sheikholeslami, M., Ambreen, T. & Shafee, A. Convective MHD flow of hybrid-nanofluid within an elliptic porous enclosure. *Phys. Lett. A* **384**(28), 126727 (2020).
- 38. Radhika, M., Punith Gowda, R. J., Naveenkumar, R., Siddabasappa, & Prasannakumara, B. C. Heat transfer in dusty fluid with suspended hybrid nanoparticles over a melting surface. *Heat Transf.* **50**(3), 2150–2167 (2021).
- 39. Hussain, M., Imran, M., Waqas, H., Muhammad, T. & Eldin, S. M. An efficient heat transfer analysis of MHD flow of hybrid nanofluid between two vertically rotating plates using Keller box scheme. *Case Stud. Therm. Eng.* 49, 103231 (2023).
- 40. Qureshi, H., Shah, Z., Raja, M. A. Z. & Khan, W. A. Stochastic analysis of the MHD flow over a stretching porous surface with variable viscosity. *Pramana* 98(4), 1–18 (2024).
- 41. Lund, L. A., Yashkun, U., & Shah, N. A. Magnetohydrodynamics streamwise and cross flow of hybrid nanofluid along the viscous dissipation effect: Duality and stability. Phys. Fluids, 35(2) (2023).
- 42. Shal, Z. et al. Design of neural network based intelligent computing for neumerical treatment of unsteady 3D flow of Eyring-Powell magneto-nanofluidic model. *J. Market. Res.* 9(6), 14372–14387 (2020).
- Zubair, M., Qureshi, H., Hussain, A., Khan, W. A. & Muhammad, T. Machine learning-based stochastic investigation of heat and momentum transfer in ternary-hybrid nanofluids with aggregation effects using artificial neural networks. J. Therm. Anal. Calorimet. 150, 1–19 (2025).
- 44. Alqahtani, A. M., Bilal, M., Ali, A., Alsenani, T. R. & Eldin, S. M. Numerical solution of an electrically conducting spinning flow of hybrid nanofluid comprised of silver and gold nanoparticles across two parallel surfaces. Sci. Rep. 13(1), 7180 (2023).
- 45. Ali, B. et al. Mixed convective flow of hybrid nanofluid over a heated stretching disk with zero-mass flux using the modified Buongiorno model. *Alex. Eng. J.* **72**, 83–96 (2023).
- 46. Qureshi, H., AI-driven analysis of buoyancy-convective flow of ternary-hybrid nanofluid in a porous medium over stretching cylinder. Nonlinear Dyn., pp.1–18 2025.
- 47. Qureshi, H., Latif, A., Athar, T., Raheem, A. and Muhammad, T., Artificial Neural Network Driven Investigation of thermal exchange through hybrid nanofluid of polymer/CNT across parallel sheets. Case Stud. Therm. Eng., p.106903 2025.
- 48. Zubair, M., Qureshi, H., Khaliq, U., Saidani, T. and Khan, W.A., Machine Learning analysis of Tangent Hyperbolic Nanofluid with Radiation and Arrhenius Activation Energy over falling cone under gravity. Partial Diff. Equ. Appl. Math., p.101280 2025.
- Khan, M. I. et al. Marangoni convective flow of hybrid nanofluid (MnZnFe₂O₄-NiZnFe₂O₄-H₂O) with Darcy Forchheimer medium. Ain Shams Eng. J. 12(4), 3931–3938 (2021).
- 50. Wong, K. V. & De Leon, O. Applications for nanofluids: Current and future. Adv. Mech. Eng. 2, 519659 (2010).
- 51. Gowtham, K. J., Gireesha, B. J. & Pavithra, C. G. Investigation of Third-Grade fluid flow in an inclined microchannel: Utilizing the Hermite wavelet technique for second law analysis. *Chem. Eng. Sci.* 300, 120646 (2024).
- 52. Keerthi, M. L., Gireesha, B. J. & Sowmya, G. Impact of shape-dependent hybrid nanofluid on transient efficiency of a fully wet porous longitudinal fin. *Arab. J. Sci. Eng.* 49(2), 2017–2026 (2024).
- 53. Gowtham, K. J., Gireesha, B. J. & Pavithra, C. G. A study of hybrid nanofluid (N i Z n F e 2 O 4+ M n Z n F e 2 O 4) in micro channel with partial slips and convective conditions: entropy generation analysis. *Int. J. Appl. Comput. Math.* 10(2), 45 (2024).
- 54. Qureshi, H., Shah, Z., Raja, M.A.Z., and Khan, W.A., Machine learning investigation for tri-magnetized Sutterby nanofluidic model with Joule heating in agrivoltaics technology. NANO 2024.
- 55. Leela, V. et al. Computational modelling and thermophysical characterization of Kelvin-Voigt fluid flow: A neural network approach. ZAMM-J. Appl. Math. Mech./Zeitschrift für Angewandte Mathematik und Mechanik 105(5), e70073 (2025).
- 56. Shilpa, B. et al. A novel machine learning approach for numerical simulation on the hybrid nanofluid flow past a converging/diverging channel: Properties of tantalum and alumina nanoparticles. *Partial Diff. Equ. Appl. Math.* 13, 101063 (2025).
- 57. Shilpa, B. et al. Exploration of Arrhenius activation energy and thermal radiation on MHD double-diffusive convection of ternary hybrid nanofluid flow over a vertical annulus with discrete heating. Case Stud. Therm. Eng. 65, 105593 (2025).
- 58. Rani, H. P., Shilpa, B., Leela, V. & Reddy, R. G. Numerical simulation and neural network model for hydromagnetic nanofluid convection in a porous wavy channel with thermal non-equilibrium model. *Phys. Scr.* **99**(11), 115219 (2024).
- 59. Shilpa, B. et al. Integrated neural network based simulation of thermo solutal radiative double-diffusive convection of ternary hybrid nanofluid flow in an inclined annulus with thermophoretic particle deposition. Case Stud. Therm. Eng. 62, 105158 (2024).

- 60. Kumar, P., Almeida, F. & Al-Mdallal, Q. Artificial neural network model using Levenberg Marquardt algorithm to analyse transient flow and thermal characteristics of micropolar nanofluid in a microchannel. *Partial Diff. Equ. Appl. Math.* 13, 101061 (2025).
- 61. Almeida, F., Kumar, P., Ajaykumar, A. R. & Nagaraja, B. Implementation of artificial neural network using Levenberg Marquardt algorithm for Casson-Carreau nanofluid flow over exponentially stretching curved surface. *Neural Comput. Appl.* 36(31), 19393–19415 (2024).
- 62. Kumar, P., Almeida, F. & Al-Mdallal, Q. Artificial neural network algorithm for time dependent radiative Casson fluid flow with couple stresses through a microchannel. *Alex. Eng. J.* 125, 167–184 (2025).
- 63. Kumar, P., Almeida, F., Nagaraja, B., Ajaykumar, A. R. & Al-Mdallal, Q. Neural network model using Levenberg Marquardt backpropagation algorithm for the prandtl fluid flow over stratified curved sheet. *IEEE Access* 12, 102242–102260 (2024).
- Kumar, P., Almeida, F., Muhammad, T. & Alghamdi, M. Surface drag optimization using ANOVA-Taguchi method for the unsteady radiative flow of dusty-trihybrid nanofluid in a microchannel emphasizing shape factor. J. Radiat. Res. Appl. Sci. 18(3), 101806 (2025).
- 65. Yusuf, A., Bhatti, M. M. & Ellahi, R. Study of ionic water/graphene nanofluids in solar panels under the effects of thermal radiation and slip conditions using experimental data. *Int. Commun. Heat Mass Transf.* 164, 108845 (2025).
- 66. Oni, M.O., Akolade, M.T., Samaila, G., Yusuf, T.S., Tijani, Y.O., Yusuf, A. and Malgwi, P.B., Theory of conjugate mixed convection flow of hybridized ethylene glycol based nanoparticles with Joule heating. *J.Therm. Anal.Calorimet.*, pp.1–13 2025.
- 67. Yusuf, A., Khan, S.U., Hassan, M., Bhatti, M.M. and Öztop, H.F., Heat transfer optimization of MWCNT-Al2O3 hybrid nanofluids under convective and irreversible effects. *J.Umm Al-Qura Univ Appl. Sci.*, pp.1–15 2025.
- 68. Qureshi, H., Rani, S., Altmeyer, S. A., Investigation of Marangoni Convective Flow of Hybrid Nanofluids in Darcy-Forchheimer Porous Medium. *J App Mat Sci & Engg Res*, 8(4), 01–14 (2024).

Acknowledgements

The research results are supported by the China/Shandong University International Postdoctoral Exchange Program. S. A. is a Serra Húnter Fellow.

Author contributions

Sebastian ALTMEYER: Conceptualization, Methodology, Investigation, Validation, Writing- Reviewing and Editing, Funding. Hamid QURESHI: Data curation, Methodology, Software, Visualization, Investigation, Writing-Original draft preparation. Muhammad ZUBAIR: Methodology, Investigation.

Funding

This work is supported by the Spanish Government under grants PID2023-150014OB-C21, PID2023-150029NB-I00 and national project J-03254.

Declarations

Competing interests

The authors declare no competing interests.

Additional information

Correspondence and requests for materials should be addressed to S.A.

Reprints and permissions information is available at www.nature.com/reprints.

Publisher's note Springer Nature remains neutral with regard to jurisdictional claims in published maps and institutional affiliations.

Open Access This article is licensed under a Creative Commons Attribution-NonCommercial-NoDerivatives 4.0 International License, which permits any non-commercial use, sharing, distribution and reproduction in any medium or format, as long as you give appropriate credit to the original author(s) and the source, provide a link to the Creative Commons licence, and indicate if you modified the licensed material. You do not have permission under this licence to share adapted material derived from this article or parts of it. The images or other third party material in this article are included in the article's Creative Commons licence, unless indicated otherwise in a credit line to the material. If material is not included in the article's Creative Commons licence and your intended use is not permitted by statutory regulation or exceeds the permitted use, you will need to obtain permission directly from the copyright holder. To view a copy of this licence, visit http://creativecommons.org/licenses/by-nc-nd/4.0/.

© The Author(s) 2025